AGU PUBLICATIONS

Geophysical Research Letters

RESEARCH LETTER
10.1002/2017GL074573

Key Points:
- Aftershock faulting mechanism diversity is enhanced for mainshock ruptures that extend across the shallow megathrust to near the trench
- Aftershock faulting mechanism diversity also increases as the mainshock magnitude approaches the largest event observed in the region
- Space-time patterns of large aftershocks for major megathrust events indicate varying spatial extent of elastic strain reduction

Supporting Information:
- Supporting Information S1
- Figure S1
- Table S1

Correspondence to:
T. Lay,
tlay@ucsc.edu

Citation:
Wetzler, N., Lay, T., Brodsky, E. E., & Kanamori, H. (2017). Rupture-depth-varying seismicity patterns for major and great ($M_w \geq 7.0$) megathrust earthquakes. *Geophysical Research Letters*, *44*, 9663–9671. https://doi.org/10.1002/2017GL074573

Received 16 JUN 2017
Accepted 17 SEP 2017
Accepted article online 21 SEP 2017
Published online 9 OCT 2017

Rupture-Depth-Varying Seismicity Patterns for Major and Great ($M_w \geq 7.0$) Megathrust Earthquakes

Nadav Wetzler[1,2], Thorne Lay[1], Emily E. Brodsky[1], and Hiroo Kanamori[3]

[1]Department of Earth and Planetary Sciences, University of California, Santa Cruz, CA, USA, [2]Geological Survey of Israel, Jerusalem, Israel, [3]Seismological Laboratory, California Institute of Technology, Pasadena, CA, USA

Abstract Large earthquakes on subduction zone plate boundary megathrusts result from intervals of strain accumulation and release. The mechanism diversity and spatial distribution of moderate-size aftershocks is influenced by the mainshock rupture depth extent. Mainshocks that rupture across the shallow megathrust to near the trench have greater intraplate aftershock faulting diversity than events with rupture confined to deeper portions of the megathrust. Diversity of intraplate aftershock faulting also increases as the size of the mainshock approaches the largest size event to have ruptured that region of the megathrust. Based on these tendencies, we identify "breakthrough" ruptures as those involving shallow rupture of the megathrust with volumetrically extensive elastic strain drop around the plate boundary that allows activation of diverse intraplate faulting influenced by long-term ambient deformation stresses. In contrast, homogeneity of the aftershock faulting mechanisms indicates only partial release of elastic strain energy and remaining potential for another large rupture.

1. Introduction

Plate convergence in subduction zones is driven by relatively steady long-term plate motions resisted by friction on the plate boundary megathrust fault. Episodic accumulation and release of elastic strain produces irregular cycles of large earthquakes (e.g., Christensen & Ruff, 1988; Dmowska & Lovison, 1992; Lay et al., 1989). The time-varying elastic strains of the boundary earthquakes superimpose on long-term elastic strains from plate deformation, modulating their seismic expression. Megathrust frictional properties appear to be heterogeneous, with patchy regions of frictional locking and stress accumulation (resulting in repeated stick-slip sliding) surrounded by regions with stable sliding (e.g., Kanamori, 2014; Lay, 2015; Scholz, 1998). Earthquake ruptures may span all or only a portion of the megathrust, with corresponding total or partial elastic strain drop in the volume around the fault (e.g., Hasegawa et al., 2012; Yang et al., 2013).

Regional interplate and intraplate seismicity varies throughout the seismic cycle (e.g., Lay et al., 1989). Commonly, regions that are strongly locked have prolonged periods with little megathrust activity in the areas where large slip will occur in a subsequent earthquake. As stress builds up to the failure limit for a locked patch, small ruptures may occur as foreshocks. After a mainshock, aftershocks nucleate nearby, either releasing residual stresses on the fault or as a result of static or dynamic stress perturbations produced by the coseismic slip. The mainshock magnitude and placement on the plate boundary is expected to determine whether the event completes the seismic cycle or only partially reduces the accumulated elastic strain.

The goal of this paper is to examine the seismicity patterns associated with large interplate subduction earthquakes to determine whether they provide a proxy for elastic strain release indicative of the mainshock's significance in the regional earthquake sequence. Previous work suggests that such a relationship may be revealed by the focal mechanism patterns where the large elastic strain accumulation around the region that slips in a mainshock inhibits diversity of faulting prior to the mainshock (e.g., Christensen & Ruff, 1988; Dmowska & Lovison, 1992; Kato & Igarishi, 2012; Lay et al., 1989). Whether this inhibition changes significantly during the mainshock may be influenced by rupture characteristics such as the depth extent of rupture and the degree of volumetric elastic energy reduction achieved during the mainshock.

We examine the variability of aftershock focal mechanisms and seismic moment rates for a range of large, interplate megathrust mainshocks. Distinct aftershock distributions suggest that some mainshocks represent completion of the regional irregular seismic cycle, resetting the elastic strain accumulation on the megathrust and allowing long-term stresses to manifest in more diverse regional faulting. We identify these events as

"breakthrough" events: shallow rupture near the free surface boundary condition results in efficient relaxation of strain in the surrounding rock volume.

2. Mainshock Selection and Spatial Windowing

Our mainshock data set comprises 101 $M_w \geq 7.0$ subduction zone plate boundary earthquakes between 1990 and 2016 that have robust seismic moments (M_0) and self-consistently determined models of coseismic slip distribution (e.g., Ammon et al., 2006; Banerjee et al., 2007; Lay et al., 2011, 2009; Miyazaki et al., 2004; Ye et al., 2016). The compilation of solutions in Ye et al. (2016) is used, so that all models are comparable with consistent parameterization and methodological choices. The slip models have uncertainties due to typical limitations of finite-fault inversions (e.g., Hartzell & Heaton, 1983; Kikuchi & Kanamori, 1991; Lay et al., 2010; Ye et al., 2016), but we do not use the details of the slip distributions beyond the general depth extent of rupture. Slip models and seismicity sequences for all mainshocks considered here are shown in supporting information Figure S1.

The slip models are used to define regions for evaluating the attendant seismicity pattern for each mainshock. We use spatial windows that scale up the rectangular mainshock slip model dimensions by ~25%; an example is shown for the 2 September 1992 Nicaragua M_w 7.7 earthquake in Figure 1. The slip model dimensions are usually already generous areas, so our expanded areas cover significant regions around the ruptures. The multiwindow inversions are not particularly sensitive to the hypocenter placement. In a handful of cases we constrain the source region to avoid adjacent large events and their aftershock sequences. To ensure that the rectangular spatial windows based on the slip models do not bias our findings, we also consider an alternate spatial windowing based on a circular crack model (Eshelby, 1957) centered on the mainshock hypocenter with radius $R_E = \left(\frac{7M_0}{16\Delta\sigma}\right)^{1/3}$, where uniform static stress drop, $\Delta\sigma = 3$ MPa, is assumed (Figures 1 and S1). Our results are not affected significantly by the particular choice of spatial windowing as demonstrated in the supporting information figures, so we present results for the rectangular source regions.

We exclude mainshocks with very close spatial or temporal proximity to preceding large magnitude earthquakes to avoid contamination of background rates by aftershock sequences. For convenience, we adopt the megathrust depth nomenclature of Lay et al. (2012), with Domain A corresponding to the shallowest portion of the megathrust extending from the trench to ~15 km depth, Domain B corresponding to 15–35 km depth range, and Domain C corresponding to depths greater than 35 km.

3. Estimating Focal Mechanism Heterogeneity

To characterize the distributions of focal mechanisms and cumulative moment-rate of each mechanism type for the seismicity before and after each mainshock within our source region search areas, we utilize all $M_w \geq 5.2$ events from the Global Centroid Moment Tensor (GCMT) catalog (http://www.globalcmt.org/CMTsearch.html) from 1976 to 2016 (e.g., Dziewonski & Woodhouse, 1983). The GCMT catalog is formally complete for $M_w \geq 5.2$ (Figure S2), but this is in terms of relative sampling across the magnitude range, not in absolute completeness. To avoid regional and time-varying biases in the GCMT centroid location estimates, we use the hypocentral estimates from the U.S. Geological Survey (USGS) Preliminary Determination of Epicenters catalog. The rupture models are positioned relative to USGS hypocenters, ensuring consistency relative to the seismicity distributions. Uncertainties in event locations are not critical for this study, as we primarily rely on focal mechanism information for grouping events.

We use four successive time windows for characterizing seismicity. The background window is defined from the beginning of the GCMT catalog in 1976 or from 14 days after the occurrence of the last prior event after 1976 with magnitude larger than 0.2 units less than the mainshock up to 60 days before the mainshock (Figure 1c). A 60 day window is used to define foreshocks (Figure 1a). A 14 day window is used to define short-term aftershocks (Figure 1b). We performed a sensitivity test of the choice of 14 day time window, using 4 and 30 days, finding that the shorter time window substantially increases the number of mainshocks having no aftershocks detected (from 17 with 14 days to 23 with 4 days), and a longer time window is less reliable for regions with high background seismicity (Wetzler et al., 2016). A long-term aftershock window extends from more than 14 days after the mainshock to the

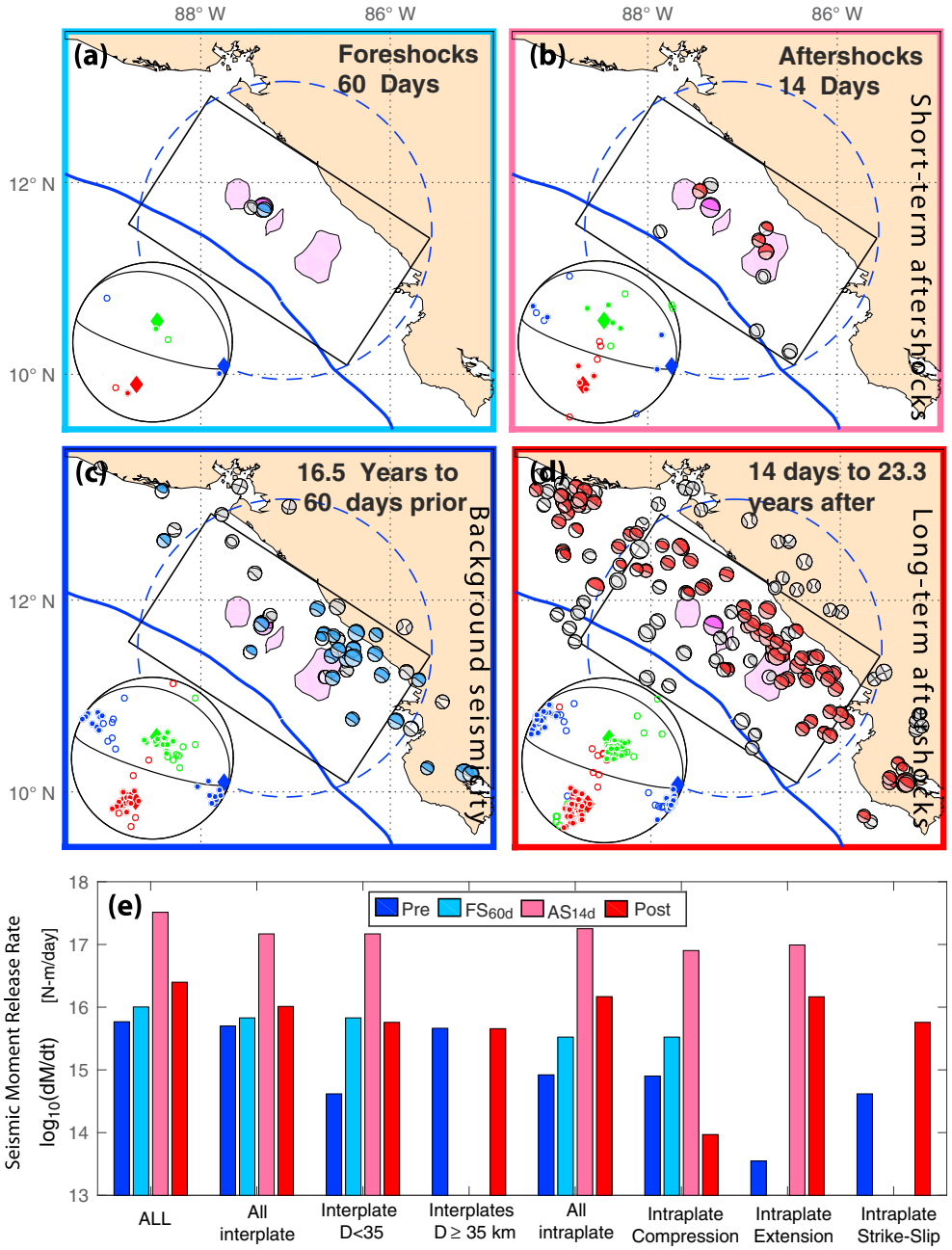

Figure 1. Seismicity sequence from the GCMT catalog prior to and following the 2 September 1992 M_w 7.7 Nicaragua earthquake for varying time intervals: (a) in the 60 days preceding the event, (b) in the first 14 days after the event, (c) from 1976 to 60 days before the mainshock, and (d) after the first 14 days to the end of 2016. Each panel includes a lower hemisphere stereographic plot of the distribution of the green compressional (*P*), red tensional (*T*), and blue null (*B*) principal stress axes of the corresponding seismicity and the mainshock (solid diamonds). Events having *P*, *T*, and *B* axes all within 30° of the mainshock values are indicated by filled color symbols and identified as interplate events. Large-slip zones (>50% of the maximum slip) are shown in pink. The mainshock mechanism is magenta, the blue-filled mechanisms are foreshocks on the megathrust, and red-filled mechanisms are aftershocks on the megathrust. The rectangular area indicates the region in which seismic moments are summed for each category of events for the four different time windows (with consistent color coding) indicted by (e) the histograms at the bottom. The blue circles are an alternate source area discussed in the text.

end of 2016 or to 60 days before the first following event with magnitude larger than 0.2 units less than the mainshock (Figure 1d). The long-term aftershock activity has magnitude varying contributions from Omori-like aftershock decay relative to background rate.

Seismicity moment rates are calculated for each of the four space-time windows for the sum of seismic moments of events with different mechanism types divided by the duration of the time windows (in days). Based on the GCMT focal mechanism of each event, two main categories are classified: interplate (shallow-dipping thrust events on/near the megathrust) and intraplate (all mechanisms off the megathrust). We assign events to these categories by comparing angles of the pressure (*P*), tension (*T*), and null (*B*) principal stress axes with those of the mainshock. Earthquakes designated as interplate are required to have all three principle stress directions (for *P*, *T*, and *B*) $<30°$ (angles between vectors) from the mainshock values (Figure 1). Interplate events are further subclassified to shallow focal depths ($\leq$35) and deeper focal depths based on the GCMT centroid depth estimates. Intraplate events are subclassified to strike-slip, normal faulting (extensional), and thrust (compressional) mechanism types (Figure 1e). Mechanism variations and moment rate variations like those in Figure 1 are determined for each event (Figure S1), and we combine the results from all events to determine the common behavior.

We find that the mainshock rupture depth extent is important for most of the systematic tendencies in our data set. We thus focus on two main depth extent subdivisions: mainshocks that rupture at least Domain A (shallow tsunami earthquakes tend to rupture entirely within Domain A, but some great ruptures such as 2011 Tohoku M_w 9.1 rupture Domains A, B, and C and they are included in this subdivision) and mainshocks that rupture just Domain B. We designate these Domain A and Domain B ruptures, respectively (we have only four events that rupture just Domain C so these are not shown separately in most figures).

4. Seismicity Moment Rate and Mechanism Patterns

One of our goals in this study is to determine whether the timing of the mainshock relative to the regional seismic behavior influences the aftershock seismicity. As a measure of this, we define a scaled magnitude, M_{Scaled}:

$$M_{\text{Scaled}} = 1 - \left(\frac{M_{\text{Max}} - M_W}{\Delta M}\right), \tag{1}$$

where M_{Max} is the maximum magnitude observed in the mainshock source area (See Table S1), M_w is the mainshock magnitude, and ΔM is the difference between maximum and minimum magnitudes of mainshocks in our catalog (2.2). The choice of M_{Max} is based on the seismically recorded events on the subduction interface of each mainshock rupture (Christophersen et al., 2015) and thus may be an underestimate of the largest possible M_w for some regions. By design, M_{Scaled} has values varying between 0 and 1, with a value of 1 indicating a mainshock at the maximum expected size for the region. As the mainshock magnitude approaches the maximum value, the region is presumably closer to completion of the local strain accumulation process, enhancing the potential regional elastic strain drop. Smaller, midcycle events will likely not achieve as extensive of strain reduction. We examine seismicity patterns as functions of M_w and M_{Scaled} to disentangle relationships that are solely a function of earthquake magnitude from those that are dependent of the evolution of the cycle.

Cumulative histograms for all mainshocks of total moment rates (Figures 2a and 2b) and event counts (Figures 2c and 2d) for the short-term (14 day) aftershock sequences for the seven different mechanism categories identified in Figure 1e display striking differences between mainshocks that rupture Domain A and Domain B. Domain A mainshocks have a much higher percentage of intraplate aftershocks both in terms of seismic moment and event numbers. Aftershocks associated with Domain B mainshocks (Figures 2b and 2d) are dominated by interplate thrust faulting activity, primarily at shallow depth. Similar histograms are found if the counts are normalized by event. Figure 1 is an example of a Domain A rupture that depicts this behavior clearly, as do the many individual event plots and histograms in Figure S1. The alternative circular seismicity search regions yield very similar cumulative histogram patterns (Figure S3). The maps in Figure S1 show all events in the map area, and it is clear that no outer rise activity is missed by the windowing for Domain B ruptures.

To evaluate changes in moment rates of different categories of events, we compute ratios of the seismic moment rates of short-term and long-term aftershocks to the background rates of similar category activity,

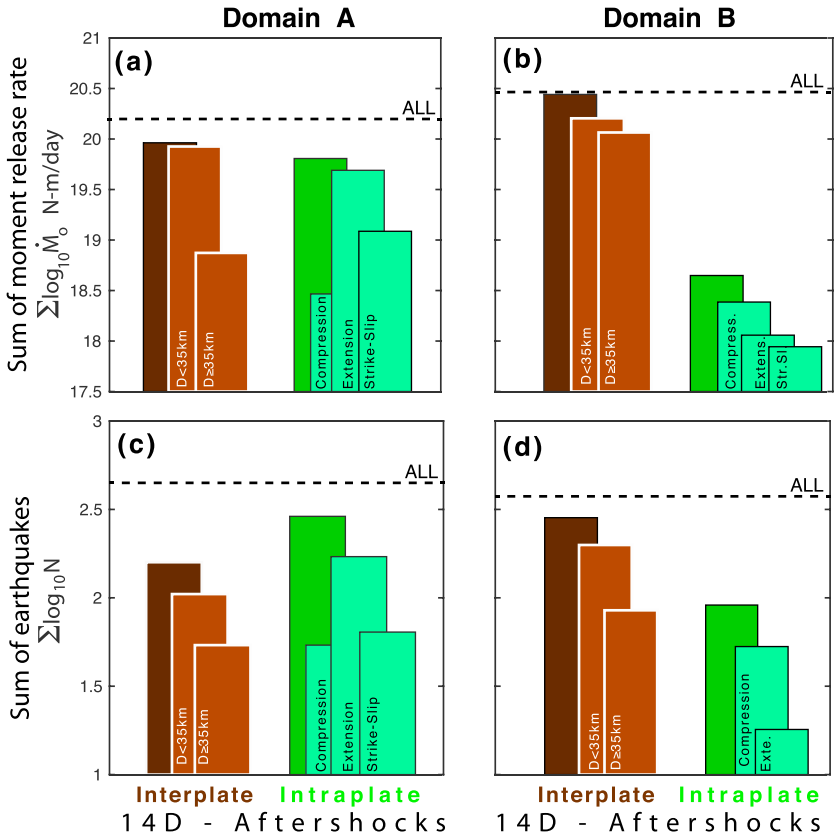

Figure 2. Cumulative (a and b) seismic moment and (c and d) number of aftershocks for 102 major and great megathrust mainshocks (Figure S1), for all events in the first 2 weeks after each mainshock in the rectangular search areas. The mainshocks are subdivided into events that rupture at least Domain A (Figures 2a and 2c) and those with ruptures confined to Domain B (Figures 2b and 2d). Interplate faulting is indicated with brown tones and intraplate activity with green tones, with distinct faulting subcategories being labeled. The dark brown and dark green histograms sum to give the level indicated by ALL in each case.

denoting these as "normalized moment rates." The normalization emphasizes the perturbation in seismicity caused by the mainshock strain drop and induced stress changes (e.g., Lin & Wu, 2012). Figure S4 shows the normalized moment rates for interplate and intraplate aftershocks, grouped by whether the mainshock ruptures Domain A or Domain B. As expected, larger mainshocks generally produce more aftershocks. While the normalized long-term rates for $M_w \leq 8$ events scatter around the background rates (ratios near 1), higher-magnitude mainshocks have relatively high rates due to their long Omori aftershock decays.

Somewhat different trends with M_{Scaled} are found. Most ruptures of Domain A tend to reset the seismic cycle (Figures S4e and S4g). Tsunami earthquakes confined to Domain A do not have observationally well-defined M_{max}, but as the slip is often quite large in these rare events, recent events are likely to be representative of the largest viable rupture near the accretionary toe. Domain B ruptures show increases in interplate seismicity rates with M_{Scaled} for the short-term and long-term aftershock seismicity (Figure S4f). For Domain B ruptures large M_{Scaled} events have higher intraplate activity (Figure S4h). Use of the circular search areas reduces some of the trends but gives similar overall patterns (Figure S5).

The distributions of fraction of intraplate seismic moment rate to total seismic moment rate for both short-term (14 day) and long-term windows show consistent differences between Domain A and B ruptures (Figure 3). Domain A ruptures activate large intraplate cumulative moment, while Domain B mainshocks activate little intraplate cumulative moment. The behavior is systematic enough that we seek a relationship between known Domain A rupturing and Domain B-only rupturing events with three observations for each event: M_{Scaled}, long-term, and short-term intraplate/total aftershock moment rates (Table S1). We designate

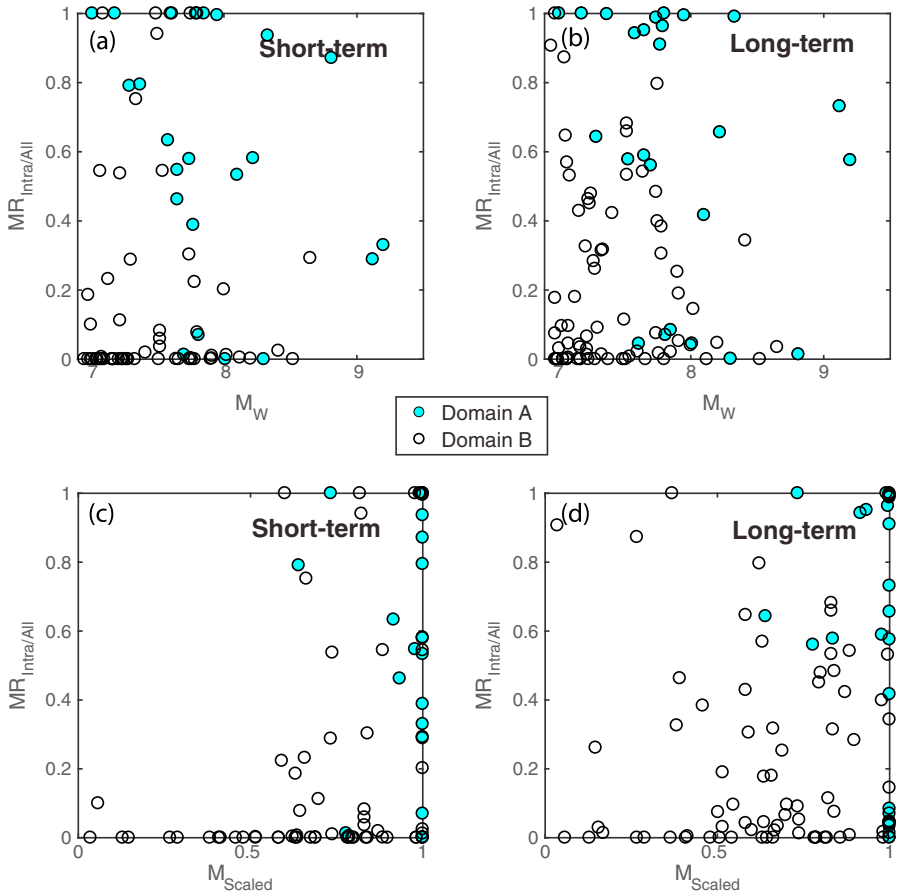

Figure 3. Distributions of the ratios of intraplate seismic moment rate to total moment seismic rate of the (a, c) short-term and (b, d) long-term time intervals plotted versus mainshock moment magnitude (Figures 3a and 3b) and M_{Scaled} (Figures 3c and 3d).

each event as a Domain A rupture (+1) or a Domain B rupture (−1) in a data vector, D, and invert for weights of the three observations and a baseline shift:

$$\hat{D} = \alpha M_{\text{Scaled}} + \beta \frac{\dot{M}^{\text{Short-term}}_{\text{Intraplate}}}{\dot{M}^{\text{Short-term}}_{\text{All}}} + \gamma \frac{\dot{M}^{\text{Long-term}}_{\text{Intraplate}}}{\dot{M}^{\text{Long-term}}_{\text{All}}} + \delta. \quad (2)$$

Positive values of the model predictions, $\hat{D}$, indicate that Domain A is predicted from the seismicity measures, and negative values indicate that Domain B is predicted. The model correctly predicts the sign of our a priori rupture designations for 93 out of 101 mainshocks (Figure 4a and Table S1), for values of α = 1.1, β = 0.7, γ = 0.9, and δ = −1.8. Similar results are obtained using the circular spatial windows (Figure 4b). The eight inconsistencies include six events designated as Domain A ruptures misclassified as Domain B, and two designated Domain B ruptures misclassified as Domain A (all are discussed in the supporting information). Of these only the 2015 Illapel, Chile, earthquake is truly anomalous; it appears to have ruptured to the trench but generated no large intraplate activity (Figure S1, event ID 100). The performance of a domain classification algorithm was not improved by applying corrections for background moment rates or by use of simple event count ratios. This analysis demonstrates that the magnitude and seismicity patterns alone provide strong guidance on the depth extent of rupture, with ruptures extending to shallow depth manifesting enhanced intraplate activity.

5. Discussion and Conclusion

The large-event seismicity patterns clearly sample a range of behavior, but it is useful to define two end-member rupture scenarios (Figure 5). The absolute and relative intraplate seismic moment rates after large

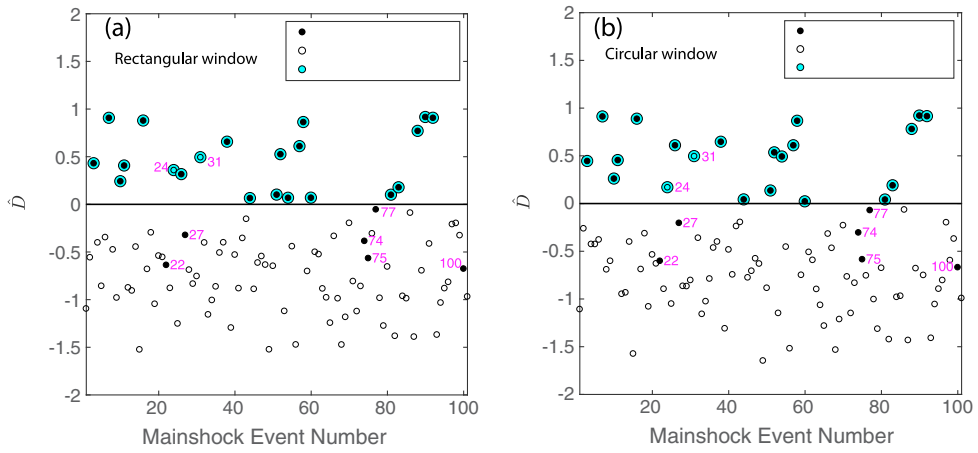

Figure 4. Predicted classification of rupture domains, $\hat{D}$ for (a) rectangular and (b) circular spatial windows. Positive values correspond with predictions of Domain A ruptures and negative values with Domain B ruptures, based on the multiparameter regression of a priori designations of Domain A or Domain B based on slip models and observed values of M_{Scaled}, long-term, and short-term intraplate/total moment rates (Figure 3). Mainshock event numbers are shown for the eight outliers (discussed in the supporting information Text S1).

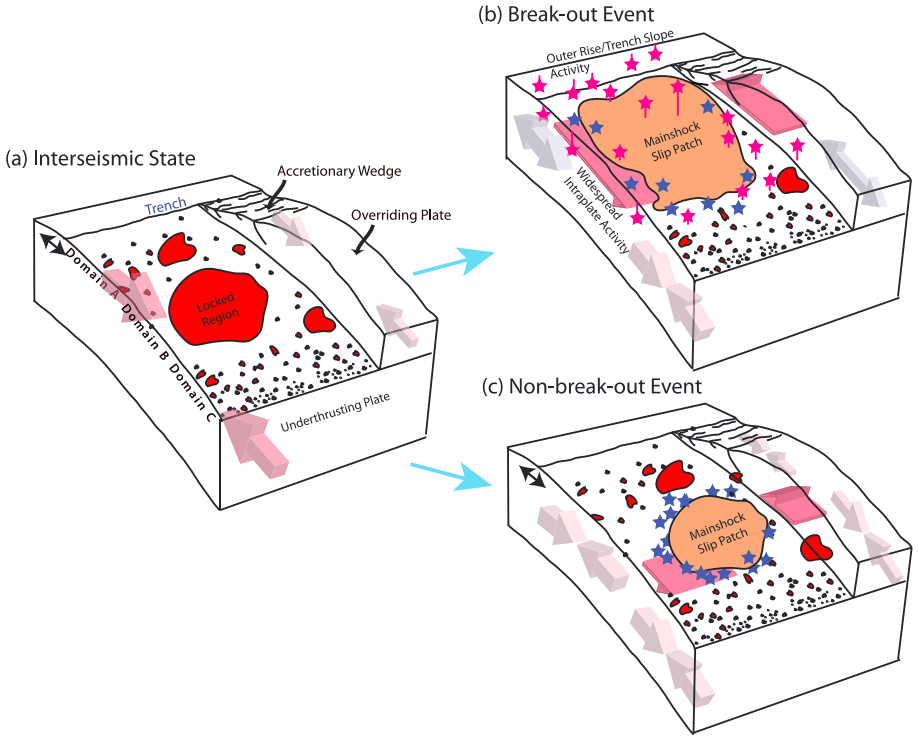

Figure 5. Schematics of a subduction zone megathrust (a) prior to failure, (b) after a shallow breakthrough event rupture, and (c) after a nonbreakthrough event rupture. Red patches are stuck patches with accumulated stress before and after rupture. Domains A, B, and C are indicated in Figure 5a, with large arrows indicating the accumulated tectonic strain in the underthrusting and overriding plates caused by frictional resistance to slip in the red patches. After rupture, the interplate aftershocks (blue stars) and intraplate aftershocks (magenta stars) indicate whether the event was a breakthrough event that ruptured through Domain A with near total tectonic shear stress and elastic strain reduction that allows broad activation of diverse aftershock faulting environments (Figure 5b) or a nonbreakthrough event that had rupture confined to Domain B (or C) (Figure 5c), leaving significant coupled regions updip and downdip of the main slip zone, and less overall elastic strain reduction, resulting in a much lower percentage of intraplate aftershock activity. Breakthrough is found for huge megathrust events and for tsunami earthquakes, with high aftershock focal mechanism diversity and intraplate faulting rate increases observed in both the short-term and long-term sequences after the mainshock (Figure 5b).

megathrust events are correlated with the depth extent and size of the mainshock rupture. Steady far-field plate motions build up the strain energy in the volume around locked regions during the interseismic period (Figure 5a). If the mainshock approaches the regional peak event size, and/or the rupture occurs just within Domain A, the postevent seismicity patterns reflect a large elastic strain energy reduction that we identify as a breakthrough event with large positive $\hat{D}$ (Figure 5b). Ruptures that extend to the trench essentially decouple the underthrusting plate from the over overriding plate, removing the time-varying confining regional compression and allowing activation of diverse intraplate faulting mechanisms, including outer rise and trench slope normal faulting associated with plate bending stresses (e.g., Christensen & Ruff, 1988) and intraslab faulting associated with slab pull (e.g., Lay et al., 1989) and upper plate extensional and strike-slip faulting. In a nonbreakthrough event, the mainshock does not rupture to shallow depth, localizing the elastic energy drop around the slip zone and regional compression is still superimposed on the four-lobed strain modulations from the faulting, inhibiting activation of intraplate faulting and resulting in predominance of interplate aftershock activity (Figure 5c). In both scenarios, stress changes from the mainshock concentrate aftershock activity on the periphery of the coseismic slip zone (e.g., Frank et al., 2017), but this is more localized and two-dimensional for the nonbreakthrough case. Numerical models of Coulomb stress changes for ruptures that do or do not reach the surface support the basic patterns noted here (e.g., Lin & Stein, 2004; Pitarka et al., 2009; Xu et al., 2016). For shallow ruptures, extensional stress produced seaward of the trench interacts with bending stresses to cause widespread normal faulting in the trench slope region. For ruptures confined to the downdip megathrust, while compressional stresses are reduced, some of the preevent compression persists, and the extensional stress environment is localized to near the rupture, not extending to the outer rise region. In some cases intraplate aftershocks following breakthrough rupture are dominated by outer rise activity, but review of all of the sequences in Figure S1 demonstrates that in general intraplate activity is enhanced all around the megathrust, including in the slab below the megathrust, in the overriding plate, and along strike.

The depth extent of the mainshock rupture appears to be the essential factor for the breakthrough scenario; even magnitude 8 events may not achieve the regional elastic strain reduction over a broad enough volume to activate extensive intraplate activity. For example, the 12 September 2007 M_w 8.5 Sumatra event (Figure S1, ID 63) ruptured only Domain B of the megathrust, leaving Domain A unruptured, resulting in exclusively interplate $M_w \geq 5.2$ aftershock activity. On the other hand, the comparable size 15 November 2006 M_w 8.3 Kuril earthquake (Figure S1, ID 58) ruptured both Domains B and A, generating intense intraplate activity. While shallow ruptures impart larger stress changes on the outer rise than deeper ruptures, the fact that all environments around the megathrust experience increased intraplate activity indicates that breakthrough rupture is fundamentally distinct from contained rupture.

Another indication of the breakthrough property of shallow ruptures is the Gutenberg-Richter *b value* calculated for the entire population of 14 day aftershock sequences grouped by Domain A ruptures (0.91) and by Domain B ruptures (0.78) (Figure S6). In general, interplate faulting localizes on an optimally oriented two-dimensional plane with respect to the regional stress field (e.g., Celerier, 2008), whereas intraplate faulting involves a three-dimensional distributions of faults that increases the range of viable geometries for smaller events resulting in higher *b* value. Thus, aftershock sequences for subduction zone breakthrough events have higher *b* values overall.

Spatiotemporal patterns of seismicity can be diagnostic of the crustal stress state, reflecting the process of interplate strain accumulation and release modulating intraplate stresses from long-term slab deformation such as bending and unbending. (Christensen & Ruff, 1988; Lay et al., 1989). Improved constraints on mainshock slip distributions now allow us to recognize the importance of depth extent of rupture. Breakthrough events that reset the elastic strain accumulation are accompanied by broad increases in intraplate activity, whereas events that rupture only the central and deeper megathrust have more localized, predominantly interplate aftershock activity, leaving residual strain that may produce additional large events, including tsunami earthquakes. Seismic hazard assessments can therefore be informed by the different patterns of aftershock activity.

Acknowledgments
This work made use of MATLAB software. The USGS National Earthquake Information Center (NEIC) and Global Centroid Moment Tensor (GCMT) earthquake catalogs provided the locations and focal mechanisms considered in this study. We thank two anonymous reviewers for their helpful comments. This work was supported by U.S. NSF grant EAR1245717 to Thorne Lay.

References

Ammon, C. J., Kanamori, H., Lay, T., & Velasco, A. A. (2006). The 17 July 2006 Java tsunami earthquake. *Geophysical Research Letters*, *233*, L234308. https://doi.org/10.10239/2006GL028005

Banerjee, P., Pollitz, F., Nagarajan, B., & Bürgmann, R. (2007). Coseismic slip distributions of the 26 December 2004 Sumatra–Andaman and 28 March 2005 Nias earthquakes from GPS static offsets. *Bulletin of the Seismological Society of America*, *97*(1A), S86–S102.

Celerier, B. (2008). Seeking Anderson's faulting in seismicity: a Centennial celebration. *Reviews of Geophysics*, *46*, RG4001. https://doi.org/10.1029/2007RG000240

Christensen, D. H., & Ruff, L. J. (1988). Seismic coupling and outer rise earthquakes. *Journal of Geophysical Research*, *93*, 13,421–13,444.

Christophersen, A., Berryman, K., & Litchfield, N. J. (2015). The GEM faulted Earth project: Version 1.0 (GEM Tech. Rep., 234 pp.). https://doi.org/10.13117/GEM.GEGD.TR2015.02

Dmowska, R., & Lovison, L. C. (1992). Influence of asperities along subduction interfaces on the stressing and seismicity of adjacent areas. *Tectonophysics*, *211*, 23–43.

Dziewonski, A. M., & Woodhouse, J. H. (1983). An experiment in systematic study of global seismicity: Centroid-moment tensor solutions for 201 moderate and large earthquakes of 1981. *Journal of Geophysical Research*, *88*(B4), 3247–3271.

Eshelby, J. D. (1957). The determination of the elastic field of an ellipsoidal inclusion, and related problems. *Proceedings of the Royal Society A Mathematical, Physical and Engineering Sciences*, *241*, 376–396.

Frank, W. B., Poli, P., & Perfettini, H. (2017). Mapping the rheology of the Central Chile subduction zone with aftershocks. *Geophysical Research Letters*, *44*, 5374–5382. https://doi.org/10.1002/2016GL072288

Hartzell, S. H., & Heaton, T. H. (1983). Inversion of strong ground motion and teleseismic waveform data for the fault rupture history of the 1979 Imperial Valley, California, earthquake. *Bulletin of the Seismological Society of America*, *73*, 1553–1583.

Hasegawa, A., Yoshida K., Asano, Y., Okada, T., Iinuma, T., & Ito, Y. (2012). Change in stress field after the 2011 great Tohoku-Oki earthquake, *Earth and Planetary Science Letters, 355–356*, 231–243. https://doi.org/10.1016/j.epsl.2012.08.042

Kanamori, H. (2014). The diversity of large earthquakes and its implications for hazard mitigation. *Annual Review of Earth and Planetary Sciences*, *42*, 7–26. https://doi.org/10.1146/annurev-earth-060313-055034

Kato, A., & Igarishi, T. (2012). Regional extent of the large coseismic slip zone of the 2011 Mw 9.0 Tohoku-Oki earthquake delineated by on-fault aftershocks. *Geophysical Research Letters*, *39*, L15301. https://doi.org/10.1029/2012GL052220

Kikuchi, M., & Kanamori, H. (1991). Inversion of complex body waves—III. *Bulletin of the Seismological Society of America*, *81*(6), 2335–2350.

Lay, T. (2015). The surge of great earthquakes from 2004 to 2014. *Earth and Planetary Science Letters*, *409*, 133–146.

Lay, T., Ammon, C. J., Hutko, A. R., & Kanamori, H. (2010). Effects of kinematic constraints on teleseismic finite-source rupture inversions: Great Peruvian earthquakes of 23 June 2001 and 15 August 2007. *Bulletin of the Seismological Society of America*, *100*, 969–994. https://doi.org/10.1785/0120090274

Lay, T., Ammon, C. J., Kanamori, H., Xue, L., & Kim, M. J. (2011). Possible large near-trench slip during the 2011 M_w 9.0 off the Pacific Coast of Tohoku earthquake. *Earth, Planets, and Space*, *63*(7). https://doi.org/10.5047/eps.2011.05.033,%20687%E2%80%93692

Lay, T., Astiz, L., Kanamori, H., & Christensen, D. H. (1989). Temporal variation of large intraplate earthquakes in coupled subduction zones. *Physics of the Earth and Planetary Interiors*, *54*, 258–312.

Lay, T., Kanamori, H., Ammon, C. J., Hutko, A. R., Furlong, K., & Rivera, L. (2009). The 2006–2007 Kuril Islands great earthquake sequence. *Journal of Geophysical Research*, *114*, B113208. https://doi.org/10.1029/2008JB006280

Lay, T., Kanamori, H., Ammon, C. J., Koper, K. D., Hutko, A. R., Ye, L., … Rushing, T. (2012). Depth-varying rupture properties of subduction zone megathrust faults. *Journal of Geophysical Research*, *117*, B04311. https://doi.org/10.1029/2011JB009133

Lin, J., & Stein, R. S. (2004). Stress triggering in thrust and subduction earthquakes and stress interaction between the southern San Andreas and nearby thrust and strike-slip faults. *Journal of Geophysical Research*, *109*, B02303. https://doi.org/10.1029/2003JB002607

Lin, J.-Y., & Wu, W.-N. (2012). Spatio-temporal distribution of seismic moment release near the source area of the 2011 Tohoku-Oki earthquake. *Earth, Planets and Space*, *64*, 1067–1075. https://doi.org/10.5047/eps.2012.04.006

Miyazaki, S., Larson, K. M., Choi, K., Hikima, K., Koketsu, K., Bodin, P., … Yamagiwa, A. (2004). Modeling the rupture process of the 2003 September 25 Tokachi-Oki (Hokkaido) earthquake using 1-Hz GPS data. *Geophysical Research Letters*, *31*, L21603. https://doi.org/10.1029/2004GL021457

Pitarka, A., Dalguer, L. A., Day, S. M., Somerville, P., & Dan, K. (2009). Numerical study of ground motion differences between buried and surface-rupturing earthquakes. *Bulletin of the Seismological Society of America*, *99*, 1521–1537. https://doi.org/10.1785/0120080193

Scholz, C. H. (1998). Earthquakes and friction laws. *Nature*, *391*, 37–42.

Wetzler, N., Brodsky, E. E., & Lay, T. (2016). Regional and stress drop effects on aftershock productivity of large megathrust earthquakes. *Geophysical Research Letters*, *43*(23), 12,012–12,020. https://doi.org/10.1002/2016GL071104

Xu, S., Fukuyama, E., Yue, H., & Ampuero, J.-P. (2016). Simple crack models explain deformation induced by subduction zone megathrust earthquakes. *Bulletin of the Seismological Society of America*, *106*, 2275–2289. https://doi.org/10.1785/0120160079

Yang, Y.-R., Johnson, K. M., & Chuang, R. Y. (2013). Inversion for absolute deviatoric crustal stress using focal mechanisms and coseismic stress changes: The 2011 M9 Tohoku-oki, Japan, earthquake. *Journal of Geophysical Research: Solid Earth*, *118*, 5516–5529. https://doi.org/10.1002/jgrb.50389

Ye, L., Lay, T., Kanamori, H., & Rivera, L. (2016). Rupture characteristics of major and great ($M_w \geq 7.0$) megathrust earthquakes from 1990–2015: I. Source parameter scaling relationships. *Journal of Geophysical. Research: Solid Earth*, *121*, 826–844. https://doi.org/10.1002/2015JB012426